Synergistic Direct-Transformation–Crystallization Mechanism in the Quartz-to-Coesite Reconstructive Transition

Di Wang(王迪)[1,2], Wei Zhang(张微)[1*], and Quan Li(李全)[1,2*]

[1]*Key Laboratory of Material Simulation Methods & Software of Ministry of Education, State Key Laboratory of High Pressure and Superhard Materials, College of Physics, Jilin University, Changchun 130012, China*
[2]*Changbaishan Laboratory, and International Center of Future Science, Jilin University, Changchun 130012, China*

(Received 12 February 2026; accepted manuscript online 18 March 2026)

Coesite, the first discovered high-pressure polymorph of silica, is one of the most robust geological indicators of ultrahigh-pressure metamorphism and hypervelocity impact events, yet its formation mechanism remains debated. Prior studies proposed that coesite is a retrograde phase crystallizing from silica melt or glass during decompression, whereas recent geological evidence revealed a direct solid-state transition pathway from quartz to coesite, leaving the underlying microscopic pathways unresolved. Here, we employ a systematic metadynamics simulation based on environment-similarity collective variables that describe the local atomic environments of silicon to uncover the quartz-to-coesite reconstructive transition. Our results confirm that the preferential transformation from quartz $(10\bar{1}1)$ plane to coesite (010) plane in the previous experimental observation is driven by an energetically favored switching process. Large-scale simulations further reveal a synergistic direct-transformation and crystallization mechanism during the quartz-to-coesite transition, explaining the origin of coesite in shocked sandstones. These results elucidate the microscopic mechanisms of the quartz-to-coesite reconstructive transition, establish a transferable framework for studying reconstructive solid-state phase transformations, and provide new insight into ultrahigh-pressure metamorphic and hypervelocity impact processes.

DOI: 10.1088/0256-307X/43/5/050703 CSTR: 32039.14.0256-307X.43.5.050703

1. Introduction. Silica, as a fundamental constituent of the Earth's crust and mantle, exhibits structural diversity that holds significant importance and indicative value for both geoscience and materials science research.[1–9] Among its many phases, coesite, the first high-pressure polymorph of silica to be identified,[1] serves as one of the most robust mineral indicators of ultrahigh-pressure metamorphism and hypervelocity impact events.[10,11] Despite this central role, the formation mechanism of coesite has remained a subject of long-standing debate since its discovery in impact rocks in the 1960s. Conventionally, coesite has been interpreted as a decompression-driven retrograde phase crystallized from silica melt or glass.[12–15] In contrast, recent geological evidence has revealed an alternative formation pathway—direct subsolidus transformation from quartz to coesite.[16–19] This interpretation is supported by frequent observations in natural occurrences of coesite occurring enclosed within quartz with the coesite (010) plane parallel to specific quartz plane families, indicating systematic topotactic orientation relationships consistent with a martensitic-like structural transition. However, glass phases were observed in the direct transformation area in natural shocked sandstones,[17] challenging the solid-state martensitic-like transition mechanism of this process. Nevertheless, the microscopic mechanism underlying this phase transition pathway remains elusive.

With its rich polymorphism, silica has long served as a prototype system for studying framework rearrangements and bonding changes under pressure and temperature.[20–25] The advancement of enhanced sampling techniques, particularly metadynamics, has enabled researchers to track complex phase transition pathways and accelerate rare events[26–35] through the explicit introduction of appropriate collective variables (CVs). However, the quartz-to-coesite transition is particularly challenging from a computational perspective. Quartz and coesite both consist of corner-sharing SiO_4 tetrahedra with indistinguishable coordination environments and similar molar volumes (compared with other high-pressure phases) and differ primarily in the topology of the tetrahedral coordination framework.[36] Conventional order parameters such as lattice parameters, global coordination numbers, or system volume, utilized to explore other high-pressure phase transitions of silica polymorphs, provide limited discriminating power along such transition pathways and are poorly suited as CVs for enhanced sampling. Consequently, elucidating this subsolidus phase transition requires the explicit definition of effective CVs capable of describing the subtle structural differences between quartz and coesite.

Here, we employ a systematic environment-similarity-based metadynamics simulation to uncover the quartz-to-coesite reconstructive transition mechanism at the atomic scale. To effectively distinguish the crystal structures of

*Corresponding authors. Email: zhangw_bxx@jlu.edu.cn; liquan777@jlu.edu.cn
© 2026 Chinese Physical Society and IOP Publishing Ltd. All rights, including for text and data mining, AI training, and similar technologies, are reserved.

quartz and coesite, we design the environment-similarity CV based on the local atomic environment of the topological structures of silicon atoms in silica. The environment similarity kernels are defined using the previously observed orientation relationships between quartz and coesite in natural shocked sandstones. Metadynamics simulations reveal that quartz undergoes a well-defined plane-switching process before transforming into coesite, thereby reconciling indistinguishable orientation relationships reported in natural samples. Our results also suggest that the pathway with $(10\bar{1}1)_{\mathrm{Qz}}\|(010)_{\mathrm{Coe}}$ orientation relationship is energetically more favorable, consistent with prior observations.[18,19] Large-scale simulations further uncover a synergistic direct-transformation and crystallization mechanism: coesite nuclei form directly within intact quartz domains while coesite subsequently crystallizes from shear-induced amorphous phases, which is consistent with the observation in shocked sandstones.[17] These findings provide microscopic comprehension of the quartz-to-coesite reconstructive transition, establish a transferable strategy for designing environment-similarity CVs for reconstructive solid–solid phase transformations, and offer new insight into ultrahigh-pressure metamorphism and hypervelocity impact processes.

2. Method. Well-tempered metadynamics (WT-MetaD)[37] simulations with adaptive Gaussians[38] are carried out using the large-scale atomic/molecular massively parallel simulator (LAMMPS) package[39] with a development version of PLUMED 2.[40] The machine learning interatomic potential using nonlinear atomic cluster expansion (ACE) is adopted to describe the interatomic forces in silica materials.[36] We adopt environment similarity as CVs[41] based on the smooth overlap of atomic positions (SOAP) kernel approach.[42] The starting point for this description is the definition of the local environment χ around an atom, and the associated local density $\rho_\chi(\boldsymbol{r})$ is written as

$$\rho_\chi(\boldsymbol{r}) = \sum_{i\in\chi} \mathrm{e}^{-|\boldsymbol{r}_i-\boldsymbol{r}|^2/2\sigma^2},$$

where $\boldsymbol{r}_i$ are the coordinates of the neighbors relative to the central atom, and σ^2 is the variance of the Gaussian functions. The difference between an environment χ and a reference environment χ_0 of the crystal that contains n reference positions $\{\boldsymbol{r}_1^0,\ldots,\boldsymbol{r}_n^0\}$ are estimated by performing the integral,

$$k_{\chi_0}(\chi) = \int \mathrm{d}\boldsymbol{r}\rho_\chi(\boldsymbol{r})\rho_{\chi_0}(\boldsymbol{r}).$$

After normalization, the kernel takes the form

$$K_{\chi_0}(\chi) = \frac{k_{\chi_0}(\chi)}{k_{\chi_0}(\chi_0)} = \frac{1}{n}\sum_{i\in\chi}\sum_{j\in\chi_0} \mathrm{e}^{-|\boldsymbol{r}_i-\boldsymbol{r}_j^0|^2/4\sigma^2}.$$

Multiple α-quartz supercells of varying sizes are constructed, with periodic boundary conditions imposed along all three directions. Details of the initial model sizes, and the parameters of metadynamics simulations are summarized in Table S1 of the Supplementary Materials (SM). The isothermal-isobaric (NPT) ensemble with Nosé–Hoover thermostat and barostat was applied in all simulations until the systems are relaxed and equilibrated to 3 GPa and 1000 K. The timestep was set to 1 fs. The machine learning structure identifier (MLSI)[43] is applied to identify local structures of silica, taking 64 atoms as the input environment size. The atoms are visualized and color-coded in OVITO[44] in order to track the structural evolution along the phase transition pathway.

3. Results and Discussion. Since a well-designed CV is essential for describing the quartz-to-coesite phase transition, we adopt the silicon skeleton in silica as the reference environment for the environment-similarity approach. This choice stems from the fact that in both quartz and coesite each silicon atom is fourfold coordinated, whereas each oxygen atom is twofold coordinated; thus, the primary structural distinction between quartz and coesite resides in the topology of the silicon sublattice, with oxygen atoms serving as bridging elements in the covalent framework of silica. Therefore, the differences in topological structure among silica polymorphs are far more pronounced than those in coordination number or volume, which justifies the use of environment similarity as an effective CV for distinguishing their structural varieties. As illustrated in Figs. 1(a) and 1(b), removing the oxygen atoms yields fourfold-coordinated silicon skeletons that preserve the topological structural features of the original quartz and coesite structures, while simultaneously avoiding significant errors in environment-similarity calculations caused by large-amplitude thermal vibrations of oxygen atoms at high temperatures, enabling a more accurate description of the silica structures. We then optimized the parameter σ used in the SOAP-based environment-similarity kernel to maximally distinguish between quartz-like and coesite-like environments. Figures 1(c) and 1(d) show the mean difference in environment-similarity between ideal α-quartz and coesite crystals referenced to thermally equilibrated α-quartz and coesite structures at 3 GPa and 1000 K, respectively. The calculation results suggest that the optimal σ value used to define the environment-similarity kernel is 0.35 for quartz and 0.30 for coesite, and these values are adopted in the subsequent metadynamics simulations.

In natural shocked sandstones, coesite occurs enclosed within quartz with the coesite (010) plane mostly parallel to the quartz $(10\bar{1}1)$ and $(\bar{1}011)$ plane families, and a few parallel to the quartz $(1\bar{3}21)$ and $(\bar{1}3\bar{2}1)$ plane families.[18,19] With the definition of the environment-similarity kernels, we perform two series of metadynamics simulations of the quartz-to-coesite transition with the orientation relationships of $(\bar{1}011)_{\mathrm{Qz}}\|(010)_{\mathrm{Coe}}$ and $(1\bar{3}21)_{\mathrm{Qz}}\|(010)_{\mathrm{Coe}}$ within the initial quartz and produced coesite structures. Figure 2(a) demonstrates the exploration process of the quartz-to-coesite transition pathway using only coesite as the reference environment with the orientation relationship of $(\bar{1}011)_{\mathrm{Qz}}\|(010)_{\mathrm{Coe}}$. Higher accumulated bias indicates deeper local minima on the free-energy surface, which represent ground-state or metastable

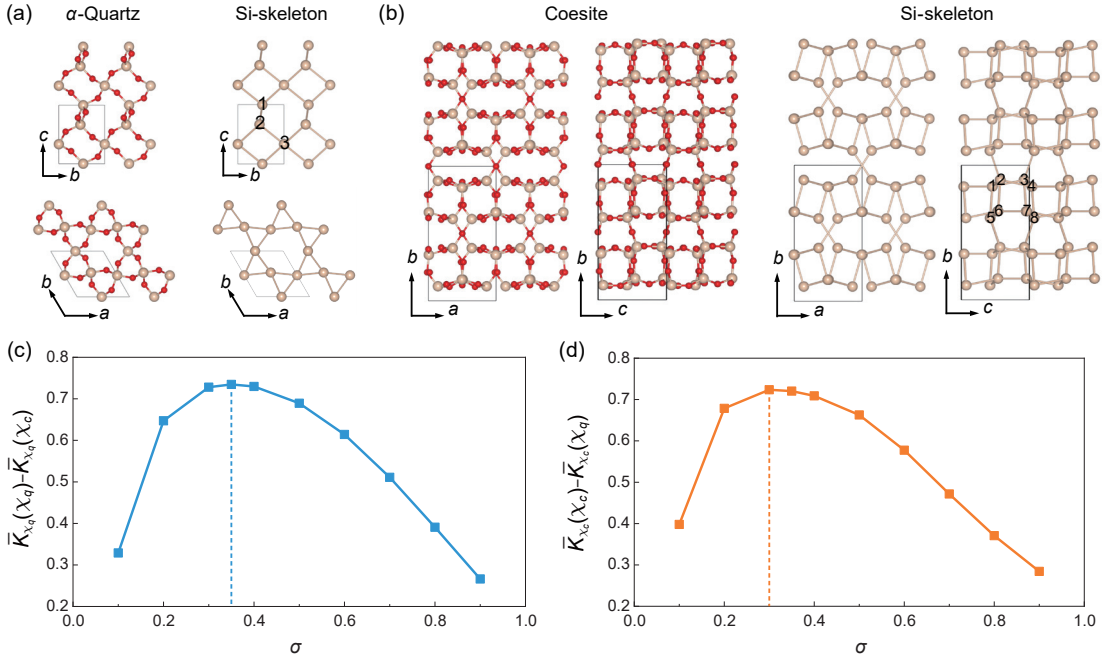

Fig. 1. Local framework environments in α-quartz and coesite and optimization of the environment-similarity kernel. (a) Crystal structure of α-quartz and the corresponding silicon skeleton viewed along different crystallographic directions. (b) Crystal structure of coesite and the corresponding silicon skeleton. Almond- and red-colored spheres denote Si and O atoms, respectively. Only Si atoms are shown in the skeleton views. Each Si atom is surrounded by four nearest-neighbor Si atoms that constitute its local environment, and the central atoms that exhibit inequivalent local environments are numbered in the silicon skeleton structures. (c) Mean difference in environment-similarity between ideal α-quartz and coesite crystals referenced to the thermally equilibrated α-quartz structure (3 GPa and 1000 K) as a function of σ. (d) Mean difference in environment-similarity for the thermally equilibrated coesite structure under the same conditions as a function of σ. Vertical dashed lines indicate the σ value chosen to maximize discrimination between quartz-like and coesite-like environments.

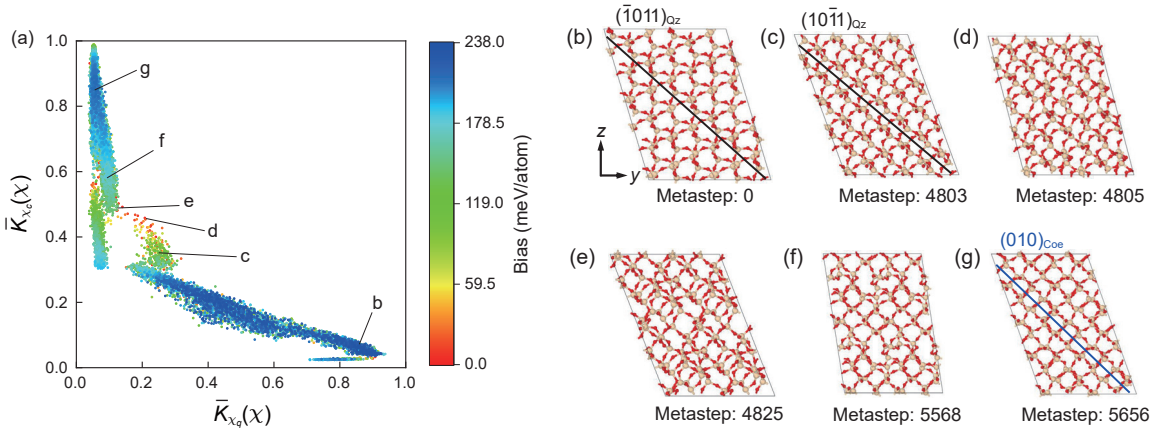

Fig. 2. Metadynamics exploration of the quartz-to-coesite transformation pathway with the quartz $(\bar{1}011)$ plane parallel to the coesite (010) plane. (a) Metadynamics trajectory projected onto the environment-similarity CVs for the quartz-to-coesite transition. The color scale denotes the accumulated bias potential. Labels b–g mark representative configurations along the pathway. (b)–(g) Snapshots of the structural evolution in a $1 \times 2 \times 2$ supercell, illustrating the progressive transition from quartz to coesite. The corresponding crystallographic planes in quartz and coesite are highlighted by black and blue lines, respectively. (d)–(f) The intermediate-state structure of this phase transition pathway.

phases. By analyzing the critical snapshots of the phase transition, a crystal-plane-switch process is captured, where the initial quartz structure [Fig. 2(b)] first undergoes structural oscillation under deformation, switching the $(\bar{1}011)$ plane to the $(10\bar{1}1)$ plane without destroying the integrity of the quartz structure, as shown in Fig. 2(c). The detailed sequence of this plane-switch process is illustrated in a clearer perspective in Fig. S1 in the SM. The length and width of the rectangular motif in quartz are mutually convertible under deformation, resulting in a crystal-plane-switch phenomenon.

The bias calculation indicates that the system remains in a low free-energy state throughout the plane-switch segment of the trajectory [between b and c in Fig. 2(a)],

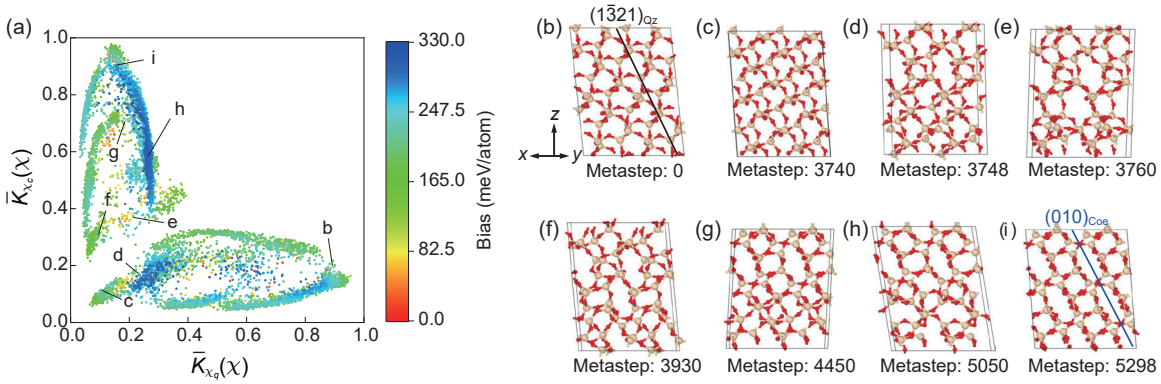

Fig. 3. Metadynamics exploration of the quartz-to-coesite transformation pathway with the quartz $(1\bar{3}21)$ plane parallel to the coesite (010) plane. (a) Metadynamics trajectory projected onto the environment-similarity CVs for the quartz-to-coesite transition. The color scale denotes the accumulated bias potential. Labels b–i mark representative configurations along the pathway. (b)–(i) Snapshots of the structural evolution in a $2\times1\times1$ supercell, illustrating the progressive transition from quartz to coesite. The corresponding crystallographic planes in quartz and coesite are highlighted by black and blue lines, respectively. (d)–(h) The intermediate-state structure of this phase transition pathway.

consistent with the quartz structure being preserved intact. These results also settle the crystallographic ambiguity in the experimentally inferred orientation relationship of the phase transition,[19] showing that the transition preferentially proceeds either along the original $(10\bar{1}1)$ plane or along the $(10\bar{1}1)$ plane generated from the $(\bar{1}011)$ plane by plane switching, which are geometrically indistinguishable in experimental characterization. After the plane switch, silicon atoms progressively rearrange toward the coesite-like silicon skeleton via successive breaking and reformation of Si-O covalent bonds [Figs. 2(d) and 2(e)]. The coesite structure is gradually constructed under shear deformation and eventually yields a coesite crystal consistent with the $(\bar{1}011)_{\rm Qz}\|(010)_{\rm Coe}$ orientation relationship [Figs. 2(f) and 2(g)]. Throughout this transition, continuous rupture and reformation of Si-O bonds lead to a direct quartz-to-coesite transformation that involves amorphous-like structures as intermediate phases. These results are consistent with recent findings that the quartz-to-coesite transition is inhibited by amorphization.[45] The plane-switch mechanism demonstrates that both the $(\bar{1}011)$ and $(10\bar{1}1)$ planes of quartz ultimately follow the same transition pathway to form the coesite (010) plane.

For the transition pathway with the orientation relationship of $(1\bar{3}21)_{\rm Qz}\|(010)_{\rm Coe}$, we employ both quartz and coesite as reference environments to improve the sampling efficiency of the metadynamics simulations. In contrast to the $(\bar{1}011)_{\rm Qz}\|(010)_{\rm Coe}$ pathway, this route cannot directly generate an ordered topological structure of coesite along the (010) plane simply through deformation-driven alignment of silicon atoms. Instead, the silicon atoms must undergo extensive bond breaking and reforming to rearrange, which gives rise to energetically favorable intermediate structures along this transition pathway. As shown in Fig. 3(a), two metastable phases (labels d and h) appear on the free-energy landscape, corresponding to Figs. 3(d) and 3(h), which present representative intermediate structures associated with lower free energy (higher accumulated bias). Notably, the structural transition in

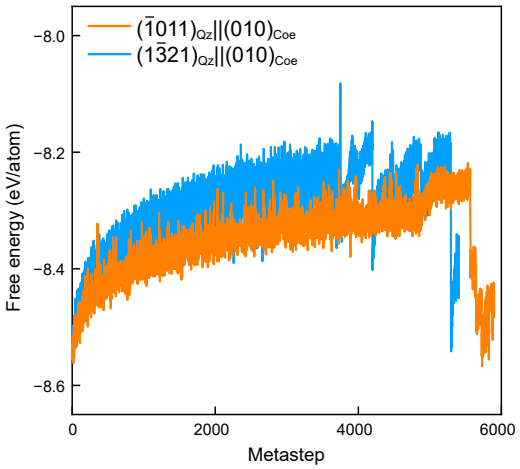

Fig. 4. Time evolution of the free energy during the quartz-to-coesite transformation from the above two simulations along two distinct transition pathways, corresponding to the orientation relationships of $(\bar{1}011)_{\rm Qz}\|(010)_{\rm Coe}$ (orange) and $(1\bar{3}21)_{\rm Qz}\|(010)_{\rm Coe}$ (blue). The free energy is plotted as a function of meta-step in the metadynamics simulations.

Fig. 3(c) also involves a crystal-plane-switch process, indicating that such plane switching is common in quartz and contributes to the diversity of orientation relationships observed in the quartz–coesite transition. We further compare the free-energy evolution of the two transition pathways. The results suggest that although the pathway with the orientation relationship of $(1\bar{3}21)_{\rm Qz}\|(010)_{\rm Coe}$ possesses transition states with lower free energy, its overall energy barrier remains higher than that of the pathway with the orientation relationship of $(\bar{1}011)_{\rm Qz}\|(010)_{\rm Coe}$ (Fig. 4). Due to the different parameters used in each metadynamics simulation (see Table S1 in the SM), the number of metadynamics steps in each phase transition pathway simulation is not comparable. This analysis rationalizes why the orientation relationships $(\bar{1}011)_{\rm Qz}\|(010)_{\rm Coe}$ and $(10\bar{1}1)_{\rm Qz}\|(010)_{\rm Coe}$ are more prevalently observed in experimental characterizations[18,19]

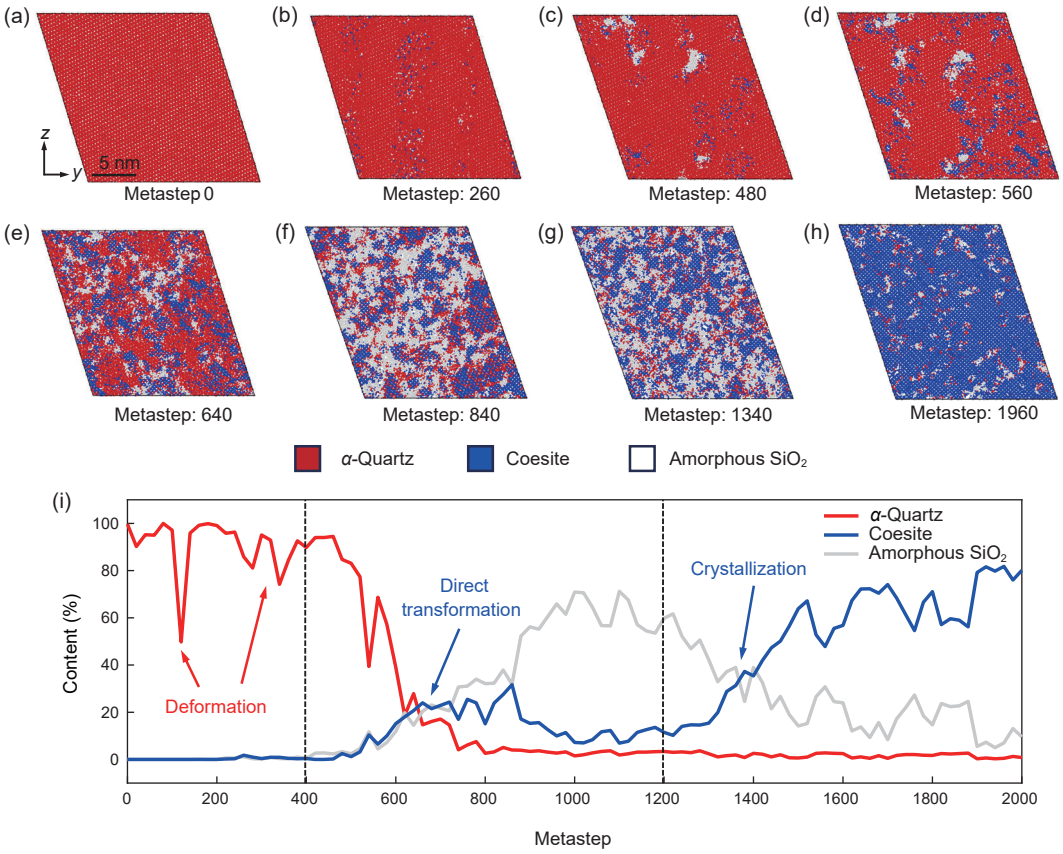

Fig. 5. Synergistic direct-transformation and crystallization during the quartz-to-coesite transition revealed by metadynamics. (a)–(h) Representative snapshots of the structural evolution along the trajectory from α-quartz to coesite. α-Quartz, coesite, and amorphous silica are colored red, blue, and white, respectively. (i) The time evolution of the content of α-quartz, coesite, and amorphous silica during the metadynamics simulation, illustrating the deformation, direct transformation, and crystallization stages.

To achieve a more realistic phase transition process from quartz to coesite, we further conduct large-scale metadynamics simulations. Figure 5(a) shows the initial quartz structure with a model size of nearly 20 nm. During the initial stage of the phase transition, the system undergoes a series of shear deformations and produces amorphous bands after the brittle failure of the quartz crystal. Figure 5(i) illustrates that the quartz content undergoes a drastic decline during the initial stage of the simulation. This corresponds to the plastic zone before brittle failure, where nearly half of the quartz fails to be identified due to severe structural deformation. Subsequently, the brittle failure enables most quartz domains to recover their original structural characteristics, accompanied by localized formation of amorphous shear bands [Fig. 5(b)]. Following the formation of amorphous bands, nucleation sites of coesite emerge within quartz [Figs. 5(c) and 5(d)]. This nucleation process originates from the direct quartz-to-coesite transformation, which generates coherently oriented coesite nuclei within the quartz matrix, thereby laying the foundation for subsequent phase transition. As shown in Fig. 5(i), a significant increase in coesite content emerges within the system after 400 meta-steps. This rise is accompanied by a substantial decrease in quartz content and progressive accumulation of amorphous structures, indicating concurrent direct transformation of quartz into both coesite and amorphous silica phases. The coesite formed via direct transformation subsequently establishes the crystalline framework within quartz through nucleation and growth processes. Figures 5(e) and 5(f) illustrate that both coesite and amorphous regions propagate through consumption of the quartz phase. Crucially, the amorphous phase here serves not as an intermediate phase for the transition but rather as an independent product distinct from the coesite framework. The coesite content undergoes a secondary increase accompanied by a reduction in amorphous silica content at 1200 meta-steps, while quartz content remains depleted [Fig. 5(i)]. These results indicate that the coesite formation now proceeds through the crystallization of the amorphous phase, with the preformed coesite framework providing seeds for the crystallization process [Fig. 5(g)].

We thus conclude that the quartz-to-coesite transition proceeds through a synergistic direct-transformation–crystallization mechanism. Specifically, deformation in quartz triggers the concurrent formation of coesite nuclei and amorphous silica phases via direct transformation, consistent with the coexistence of coesite and silica glass documented in natural shocked sandstones. In this scenario, the phase transition is synergistically driven

by direct transformation (coesite nucleation) and subsequent crystallization of the surrounding amorphous silica (coesite growth). As shown in Fig. 5(h), the resulting coesite structure exhibits a uniform crystallographic orientation with defects, providing strong evidence for a direct solid-state transformation pathway that is distinct from high-temperature recrystallization. Based on our simulation results of the synergistic direct-transformation and crystallization mechanism in the quartz-to-coesite transition, we reveal that the formation of natural coesite originates from the following process: after coesite nuclei formation via direct transformation, amorphous silica continuously crystallizes onto these nuclei. Due to coesite nuclei formed through direct transformation from the parent single-crystal quartz inheriting a uniform crystallographic orientation, the growing nuclei eventually become interlinked to form the skeletal framework of coesite. This framework consumes the surrounding amorphous silica, producing coesite crystals through crystallization with defects. In this phase transformation process, the amorphous phase is not an intermediate state but rather a stable product that synergistically facilitates the progression of the phase transition, which explains why glass phases can be observed in the direct transformation area of shocked sandstones.[17] These results suggest that amorphization of silica during the solid-state quartz-to-coesite transition is energetically more favorable than the previously proposed martensitic-like pathway and that the coesite nuclei formed via direct transformation act as a ground-state phase and seeds for crystallization. The synergistic direct-transformation–crystallization mechanism simultaneously ensures the orientation relationship of solid-state direct transformation and explains the existence of amorphous phases, thus fully conforming to natural observational results.

4. Conclusions. In summary, by defining environment-similarity kernels based on the local atomic environments of the silicon skeleton in the silica structures, we uncover the microscopic dynamics of the solid-state transition from quartz to coesite via metadynamics simulations. Our results demonstrate that the quartz-to-coesite transition preferentially proceeds by converting the quartz $(10\bar{1}1)$ plane into the coesite (010) plane, which exhibits the lowest free-energy barrier and is consistent with experimentally observed orientation relationships. The crystal-plane-switch process identified in quartz provides additional quartz–coesite orientation variants for phase transition progression, while revealing that each set of crystal planes actually undergoes a uniform transformation pathway. Large-scale simulations further uncover a synergistic direct-transformation–crystallization mechanism. In this mechanism, crystal deformation in quartz generates coesite nuclei and amorphous silica via direct solid-state transformation, and subsequent crystallization of the amorphous silica promotes the growth and coalescence of the coesite nuclei, ultimately leading to the formation of coesite. This staged process allows the amorphous silica phase to be observed in the direct transformation area of quartz and coesite in natural occurrences. These findings elucidate the microscopic mechanisms of the quartz-to-coesite phase transition, bearing profound scientific implications for understanding ultrahigh-pressure metamorphic processes and hypervelocity impact events, while providing a novel perspective for reconstructive solid-state phase transition research.

Acknowledgements. This work was supported by the National Key Research and Development Program of China (Grant Nos. 2023YFA1406103 and 2021YFA1400503), the National Natural Science Foundation of China (Grant nos. T2325013, 52288102, 52090024, and 12034009), and the Program for Jilin University (JLU) Science and Technology Innovative Research Team. We thank Dr. Hui Liang for helpful discussions.

References

[1] Coes L 1953 *Science* **118** 131
[2] Stishov S M and Popova S V 1961 *Geochemistry* **10** 923
[3] Hemley R J, Jephcoat A P, Mao H K, Ming L C, and Manghnani M H 1988 *Nature* **334** 52
[4] Teter D M, Hemley R J, Kresse G, and Hafner J 1998 *Phys. Rev. Lett.* **80** 2145
[5] Liu C, Wang J, Deng X, Wang X, Pickard C J, Helled R, Wu Z, Wang H T, Xing D, and Sun J 2022 *Chin. Phys. Lett.* **39** 076101
[6] Tian Y, Yuan X, Hu D, Zheng W, and Han W 2020 *Chin. Phys. Lett.* **37** 106101
[7] Su R, Zhang H, Han W, and Chen J 2015 *Chin. Phys. Lett.* **32** 107803
[8] Sharp T G, Goresy A, Wopenka B, and Chen M 1999 *Science* **284** 1511
[9] Miyahara M, Kaneko S, Ohtani E, Sakai T, Nagase T, Kayama M, Nishido H, and Hirao N 2013 *Nat. Commun.* **4** 1737
[10] Chopin C 2003 *Earth Planet. Sc. Lett.* **212** 1
[11] Chao E C, Shoemaker E M, and Madsen B M 1960 *Science* **132** 220
[12] Stöffler D and Langenhorst F 1994 *Meteorit. Planet. Sci.* **29** 155
[13] Chen M, Xiao W, and Xie X 2010 *Earth Planet. Sci. Lett.* **297** 306
[14] Jaret S J, Phillips B L, King Jr D T, Glotch T D, Rahman Z, and Wright S P 2017 *Meteorit. Planet. Sci.* **52** 147
[15] Stähle V, Altherr R, Koch M, and Nasdala L 2008 *Contrib. Mineral. Petrol.* **155** 457
[16] Kieffer S W, Phakey P P, and Christie J M 1976 *Contr. Mineral. and Petrol.* **59** 41
[17] Folco L, Mugnaioli E, Gemelli M, Masotta M, and Campanale F 2018 *Geology* **46** 739
[18] Campanale F, Mugnaioli E, Folco L, Gemmi M, Lee M R, Daly L, and Glass B P 2019 *Geochim. Cosmochim. Acta* **264** 105
[19] Campanale F, Mugnaioli E, Gemmi M, and Folco L 2021 *Sci. Rep.* **11** 16011
[20] Martoňák R, Donadio D, Oganov A R, and Parrinello M 2006 *Nat. Mater.* **5** 623
[21] Martoňák R, Donadio D, Oganov A R, and Parrinello M 2007 *Phys. Rev. B* **76** 014120
[22] Hu Q Y, Shu J F, Cadien A, Meng Y, Yang W G, Sheng H W, and Mao H K 2015 *Nat. Commun.* **6** 6630
[23] Liang H, Wang D, Xu R, Chen H, Zhou D, Zhang Y, and Li Q 2026 *Matter Radiat. Extremes* **11** 017802
[24] Chen H, Zhou D, Xu Y, and Li Q 2025 *Chin. Phys. Lett.* **42** 067301

[25] Liu C, Shi J, Gao H, Wang J, Han Y, Lu X, Wang H T, Xing D, and Sun J 2021 *Phys. Rev. Lett.* **126** 035701

[26] Laio A and Parrinello M 2002 *Proc. Natl. Acad. Sci. U.S.A.* **99** 12562

[27] Martoňák R, Laio A, and Parrinello M 2003 *Phys. Rev. Lett.* **90** 075503

[28] Behler J, Martoňák R, Donadio D, and Parrinello M 2008 *Phys. Rev. Lett.* **100** 185501

[29] Bonati L and Parrinello M 2018 *Phys. Rev. Lett.* **121** 265701

[30] Zhang S, Hu J, Sun X, Deng J, and Niu H 2025 *Phys. Rev. Lett.* **134** 204101

[31] Niu H, Yang Y I, and Parrinello M 2019 *Phys. Rev. Lett.* **122** 245501

[32] Tong Q, Luo X, Adeleke A A, Gao P, Xie Y, Liu H, Li Q, Wang Y, Lv J, Yao Y, and Ma Y 2021 *Phys. Rev. B* **103** 054107

[33] Santos-Florez P A, Yanxon H, Kang B, Yao Y, and Zhu Q 2022 *Phys. Rev. Lett.* **129** 185701

[34] Deng J, Hu J, Shi Y, Lee J, Niu H, and Stixrude L 2026 *Nature* **650** 361

[35] Ma X, Wang D, Lian M, Wang X, You C, Ge Y, Sun G, Liu H, Hou Y, Tao Q, Li Q, and Cui T 2025 *Sci. Adv.* **11** eaea3692

[36] Erhard L C, Rohrer J, Albe K, and Deringer V L 2024 *Nat. Commun.* **15** 1927

[37] Barducci A, Bussi G, and Parrinello M 2008 *Phys. Rev. Lett.* **100** 020603

[38] Branduardi D, Bussi G, and Parrinello M 2012 *J. Chem. Theory Comput.* **8** 2247

[39] Phimpton S 1995 *J. Comput. Phys.* **117** 1

[40] Tribello G A, Bonomi M, Branduardi D, Camilloni C, and Bussi G 2014 *Comput. Phys. Commun.* **185** 604

[41] Piaggi P M and Parrinello M 2019 *J. Chem. Phys.* **150** 244119

[42] Bartók A P, Kondor R, and Csányi G 2013 *Phys. Rev. B* **87** 184115

[43] Erhard L C, Utt D, Klomp A J, and Albe K 2024 *Model. Simul. Mater. Sci. Eng.* **32** 065029

[44] Stukowski A 2010 *Model. Simul. Mater. Sci. Eng.* **18** 015012

[45] Deng P, Hou R, Zhao Y L, and Zhu S C 2026 *Chin. J. High Press. Phys.* **40** 010103 (in Chinese)